Formation of Oriented Nanostructures from Single Molecules of Conjugated Polymers in Microdroplets of Solution: The Role of Solvent

Pradeep Kumar,[†] Adosh Mehta,[‡] Shannon M. Mahurin,[§] Sheng Dai,[§] Mark D. Dadmun,[†] Bobby G. Sumpter,[⊥] and Michael D. Barnes*[,§]

Department of Chemistry, University of Tennessee, Knoxville, Tennessee 37916; Life Sciences Division, Oak Ridge National Laboratory, Oak Ridge, Tennessee 3783; Chemical Sciences Division, Oak Ridge National Laboratory, Oak Ridge, Tennessee 37831; and Computer Sciences and Mathematics Division, Oak Ridge National Laboratory, Oak Ridge, Tennessee 37831

Received June 1, 2004

ABSTRACT: We examine the role of solution-phase polymer geometries on the favorability of forming oriented nanostructures from single conjugated polymer molecules formed from microdroplets of ultradilute solution. To our knowledge, this is the first time single molecule fluorescence correlation spectroscopy has been used to extract structural information from solution-phase fluorescence measurements. We find that production of oriented species is strongly favored in "poorer" solvents, where the polymer chains have more compact solution-phase structures. While charging during droplet generation is essential for orientation, we conclude that most of the internal organization associated with these interesting structures takes place in solution, independent of the droplets.

Introduction

Since the first report of polymer LED fabrication,[1] poly(phenylenevinylene) (PPV) and its soluble derivatives have received a great deal of attention in polymer-based optoelectronic devices.[1−5] When functionalized with flexible side groups, PPV is soluble in many organic solvents and can be easily processed into low cost and large area thin films for device applications. The soluble derivatives poly[2-methoxy-5-(2′-ethyl-hexyloxy)-1,4-phenylenevinylene] (MEH-PPV) and poly[2-methoxy-5-(2′-ethylhexyloxy)-1,4-(cyanovinylene)phenylene] (CN-PPV) are particularly attractive because of their commercial accessibility, efficient luminescence, and convenient solution processing. It has long been recognized that the photophysical properties of these polymers depend strongly on chain morphologies and their local environment.[6−13] For example, MEH-PPV is known to have different photoluminescence (PL) spectral maxima in different solvents and in solid phase. These shifts in the PL maximum are attributed to different polymer chain morphologies in different local environments.[6,8−10] The PL maximum in solutions is blue-shifted relative to that in the solid phase, and the PL maximum in a "good" solvent (where the polymer chain approximates a random coil) is blue-shifted relative to that in a poor solvent.[6,10,12]

The luminescence and photophysical properties of MEH-PPV and CN-PPV are well studied and chronicled in the literature.[7,10,14] These polymers typically have a broad absorption and emission spectra. The absorption maximum is centered approximately at 490 nm, and the emission maxima are observed at ∼575 and 600 nm. The broad absorption and emission spectra are attributed to the presence of a large number of conjugated segments that can act as local chromophores within individual polymer chains. The presence of twists, kinks, and tetrahedral defects in the polymer backbone results in a distribution of chromophore lengths, with a typical chromophore comprised of 10−15 monomer units.[15] Typically a polymer chain with a molecular weight of 100 kg/mol can have 50−80 chromophores/molecule. Since the polymer chain conformations affect the absorption and emission of the polymer, the absorption and emission maxima were found to shift in various solvents and in the bulk solid.[16]

In the solid phase and in "poor" solvents, that is, solvents that result in compact polymer chain conformations,[7,9] effects of $\pi-\pi$ overlap between conjugated segments of the same or different polymer chains manifest in spectral red shifts as well as nonlinear optical effects.[17] In PL spectral measurements of MEH-PPV in dilute solutions of chlorobenzene (CB) and tetrahydrofuran (THF), for example, Schwartz and coworkers[10] have observed a significant red shift in CB relative to THF, a result consistent with light scattering data[10] that points to a more extended polymer chain conformation of MEH-PPV in CB relative to that in THF solution. That is, $\pi-\pi$ overlap between the conjugated segments (chromophores, mostly from different polymer chains) in CB is considerable as compared to that in THF, and as a consequence the PL maximum is red-shifted in CB compared to that in THF.

In recent years, single molecule studies of MEH-PPV and similar polymers have improved the understanding of the relationship between their photophysics and chain morphology.[5,18−21] Tolbert et al.[5] investigated luminescence of MEH-PPV embedded in channels of mesoporous silica to demonstrate the intermolecular energy transfer between chromophores in a conjugated polymer chain. They observed that the transition dipole moment was oriented along the axis. Since the transition dipole moment of the ^1B_u exciton is polarized collinear with the conjugation axis,[22] polymer chains inside the channels were oriented along the pore axis. They found that

[†] University of Tennessee.
[‡] Life Sciences Division, Oak Ridge National Laboratory.
[§] Chemical Sciences Division, Oak Ridge National Laboratory.
[⊥] Computer Sciences and Mathematics Division, Oak Ridge National Laboratory.
* To whom correspondence should be addressed. Present address: Department of Chemistry, University of Massachusetts, Amhrest, MA 01003.

10.1021/ma048917w CCC: $27.50
Published on Web 07/16/2004

the energy migrates from the segments outside the channels to that trapped in the channels very rapidly. The energy migration along the chromophores inside the channels was less efficient. The increased efficiency of energy transfer outside the channels stems from the tendency of the conjugated segments to stack together (where as the chain is confined inside the silica channels) to lower their free energy. Barbara et al.[20] have combined single molecule studies with Monte Carlo (MC) simulations to model chain conformations of isolated, single molecules of MEH-PPV. The MC simulations suggest that the polymer molecules exhibit varying degrees of polarization anisotropy that depend on the chain conformation. Compared with MC calculation, polarization anisotropy measurements carried out on single molecules of MEH-PPV dispersed in a polymer matrix yielded a broad distribution of chain conformations that were correlated with a mixture of random-coil-like geometries and weakly aligned so-called "defect-cylinder" structures.[20] Although highly ordered cylindrical "rod" geometries were considered, to our knowledge no experimental evidence of these interesting species has been reported in thin film formats.

In addition to polarization anisotropy measurements, other novel optical techniques can be used to interrogate molecular structure and the local nature of radiative recombination within a single polymer chain. Recently, Huser et al. have observed nonclassical photon statistics, indicative of luminescence originating from 2 to 3 (on average) chromophoric sites, from MEH-PPV single molecules prepared from specific solvents.[23] This unique quantum optical signature was observed from samples prepared from toluene, while almost classical behavior was seen from single molecules prepared from chloroform. This showed that polymer chains isolated from so-called "good solvents", where the chain configuration is expected to approximate a random coil, exhibit photophysical behavior representative of a multichromophoric system. Single molecule studies of conjugated polymers in the absence of a support−polymer matrix are challenging due to the poor photostability of conjugated polymers in the presence of oxygen. Furthermore, the effect of the host polymer on the photoluminescence may not be understood. Understanding the photophysical properties of single conjugated polymer chains in the absence of a host polymer matrix (or substrate interactions) is often difficult due to the poor photostability of single conjugated polymer molecules in neat films.

Recently we have reported the observation of uniformly oriented luminescent nanostructures from single polymer chains of MEH-PPV isolated using microdroplet techniques.[24,25] Our experiments were carried out under ambient conditions without any supporting polymer matrix (to enhance the photostability). Fluorescence emission pattern imaging coupled with polarization anisotropy measurements indicated that these species had an intramolecular organization, with the conjugated segments aligned along the *z*-direction. The "doughnut"-like spatial luminescence intensity patterns illustrated in Figure 1 can be understood as a cylindrically folded nanostructure with conjugated segments oriented perpendicular to the glass surface. The photophysical properties of these *z*-oriented species are profoundly modified with respect to their well-studied thin-film counterparts. We have observed enhanced photostability, narrow spectral bandwidth, and near-unity contrast in polarization-modulated luminescence and photon

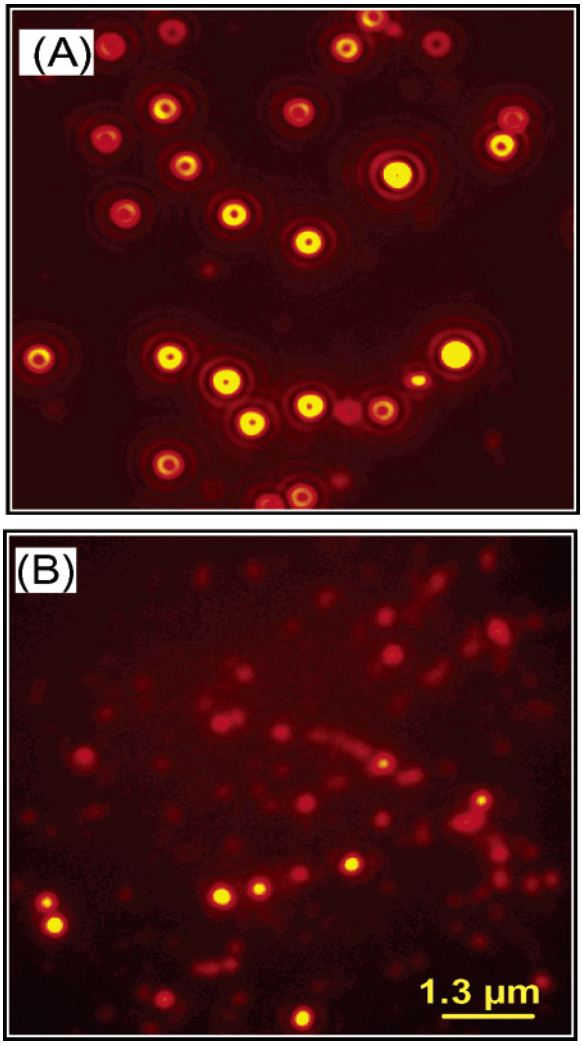

Figure 1. Fluorescence emission pattern images of (A) CN-PPV single molecules prepared by nebulization from toluene and (B) dichloromethane solutions. The "doughnut"-like patterns in (A) are indicative of single dipole emitters oriented perpendicular to the substrate. The in-focus diffraction-limited spots in (B) are indicative of random orientation of dipoles within single polymer molecules.

antibunching,[24−26] suggesting an extraordinary degree of intramolecular order. As we show by surface potential imaging of the cylindrical structure, the orientation mechanism is believed to be electrostatic in nature where excess negative charges (induced during droplet production) that have remained on the particle after solvent evaporation interact with nonprotonated SiO^- groups on the glass surface, thus orienting the long axis perpendicular to the substrate. This was confirmed by the absence of oriented structures when the glass surface was protonated as well as for conducting surfaces where image charge interactions favor in-plane orientation.

In this paper we consider the role of solvent on the formation of oriented nanostructures, their luminescence properties, and photostability of single molecules of MEH-PPV and CN-PPV prepared by microdroplet techniques. Nebulized samples from toluene, tetrahydrofuran, and dichloromethane were examined for the presence of *z*-oriented structures, and (dry state) images were correlated with solution-phase hydrodynamic radii measured by fluorescence correlation spectroscopy (FCS). We find that the formation of *z*-oriented species is

strongly favored from those solvents where the polymer chain conformations are more compact. We also carried out molecular dynamics simulation to study the effect of solvent on forming these collapsed structures. The results indicate that under most sample preparation conditions individual polymer chains are quenched in conformations that closely approximate their solution-phase geometries, and the role of droplet is crucial in inducing negative charge on the nanostructure, resulting in the orientation of the molecule.

Experimental Section

Materials. MEH-PPV (M_w = 275 000 and 132 500 g/mol) and CN-PPV (M_w = 100 000 g/mol) were obtained from Sigma Aldrich and H.W. Sands Corp., respectively, and was used without further purification. Tetrahydrofuran (THF), dichloromethane (DCM), and toluene were obtained from EM Sciences. All the solvents were of OmniSolv (HPLC) grade and were used without further purification. Fisher*finest* Premium Cover Glass (precleaned) was used as the substrate and obtained from Fisher Scientific. The cover glasses were used without further cleaning.

Sample Preparation. In our previous work, single polymer molecules (MEH-PPV or CN-PPV) were isolated from dilute solutions ($\sim 10^{-12}$ M) of THF using a piezoelectric microdroplet generator. At this nominal polymer concentration, and a 10 μm (upper estimate) droplet diameter, the average number of polymer chains per droplet is ≤ 0.3, suggesting that the probability of forming multiple-chain aggregates was negligible. The droplets, produced at a rate of $\approx$20 Hz, dried en route to the substrate in a 15 cm vented Pyrex tube with a grounded copper sleeve inside the glass tube to eliminate electrostatic interactions between the (charged) nanoparticles and stray charges on the glass tube. In this mode of production, nanoparticle samples typically show a very high degree of orientational uniformity, however, at the expense of particle collection times that range from 1 to 10 h depending on the desired coverage. We have recently found that nebulization of dilute polymer solutions using a high-pressure flow of dry nitrogen over a drawn capillary is quite satisfactory for preparing similarly oriented fluorescent nanostructures. In many cases, the nebulized samples show considerable "contamination" from in-plane or unoriented species, but with the advantage of significantly reduced sample preparation time (typically a few minutes).

In this method a Pyrex tube (10 cm in length and 3 mm in diameter) was drawn on one end and was ground to yield an orifice of $\approx$25 μm. The Pyrex tip was cleaned by sonication in THF. The open (nontapered) end of the Pyrex tube was immersed in the polymer solution. A high-pressure flow of high-purity dry N_2 was used to nebulize the solution. Varying the orifice diameter and gas velocity can control the droplet size. A cover glass was held at a distance of 15−20 cm (the distance varies depending on the vapor pressure of the solvent) away from the nitrogen nozzle and perpendicular to the flow direction. The nebulization was typically carried out for 30−45 s. Particle coverage was dependent on nebulization time and polymer solution concentration. The droplet size, polymer concentrations, and the distance between the substrate and the Pyrex tube were varied, and we observed that orientational purity was only weakly dependent on droplet size. Samples were prepared under the same conditions, including the same sample−substrate distance, gas velocity, deposition time, temperature, and humidity.

Fluorescence Imaging. Dipolar emission pattern imaging was carried out using an inverted fluorescence microscope (Nikon Eclipse TE300). Samples were illuminated with an intraobjective total internal reflection geometry, where the laser (Ar^+ laser, 514.5 nm) beam was aligned off-axis in a "top-to-bottom" sense relative to the viewer;[27] in this configuration, a vertically polarized input (TM polarization) generates a nonzero *z*-component (along with predominantly y component) of the evanescent field, allowing for simultaneous excitation of all possible transition dipole orientations with similar efficiency. Sample luminescence was imaged using a 1.4 NA 100× objective and thermoelectrically cooled back-illuminated frame transfer CCD camera (Princeton Instruments EEV-57) along with a 2× expander to give a real-space distance per pixel of 56 nm. Fluorescence was imaged through a dichroic filter and Corning long pass filter (590LP) or Omega band-pass filter (605DF35). Illumination intensities of 1 kW/cm^2, typical for most experiments, were found to be sufficient to saturate the absorption for the species of interest. All imaging experiments described here were carried out under ambient conditions in the presence of oxygen.

Fluorescence emission spectra of single molecules (in the dry state) were acquired using a Holospec f/2.2 VPT spectrograph (Kaiser Optics Inc.) with a thermoelectrically cooled CCD camera (Princeton Instruments). Single molecule emission was alternately diverted through the side port of the microscope for spectral analysis or the top port for imaging so that individual nanoparticle spectra could be registered with a specific fluorescence images to correlate spectra with dipole orientation. The spectra of individual single molecules were acquired using integration time of 10 s. After background subtraction the spectra were plotted, and the total area under the curve was obtained to get the total photon counts. Polymer samples were prepared from toluene and THF solutions were investigated.

Atomic Force Microscopy (AFM). Nanoparticle size measurements were carried out using a modified Bioscope atomic force microscope (Digital Instruments, Santa Barbara, CA) using a Nanoscope III controller. Since the AFM scanner was positioned on top of the sample, this allowed simultaneous fluorescence and topographic measurements on the same sample. Correlation of the topographic and fluorescence image was done using techniques described previously.[28] Electric force microscopy experiments were carried out on a Dimension 3100 AFM (Digital Instruments) using MESP cantilever tips, coated with cobalt (1 nm) and chromium (10 nm) (Veeco Probes, Santa Barbara, CA). The biased metal-coated AFM tip was scanned in interleave mode over the charged samples using lift heights ranging from 10 to 30 nm. The long-range electrostatic forces experienced by the oscillating cantilever were measured by monitoring the shift in cantilever frequency as it scanned over the sample.

Results and Discussion

Solvent Dependence on Chromophore Orientation. Parts A and B of Figure 1 show high-spatial resolution fluorescence images of CN-PPV prepared from toluene (relative polarity = 0.099) and DCM (relative polarity = 0.309), respectively, for similar substrate, droplet size, rare-gas pressure, polymer concentration, and sample collection time. The uniform "doughnut"-like spatial intensity patterns seen in Figure 1A are characteristic of single dipole emitters oriented perpendicular to the substrate, where the emission takes place a sine-squared angular distribution with respect to the dipole axis.[27] It is important to note that the emission pattern does not represent the actual size of the molecule under investigation or morphology, only the antenna image.

Samples in Figure 1A showed characteristics of single fluorescent molecules, like on−off blinking and discrete photobleaching. The most confirmative evidence comes from the observation of photon antibunching[26] from *z*-oriented CN-PPV nanostructures. To establish the correlation between the morphologies of single polymer chains in solution and in the dry state, we have used emission pattern imaging of the dry samples and FCS measurement in the solutions, from which the samples were prepared. The central question we are trying to address is the role of the (evaporating) microdroplet

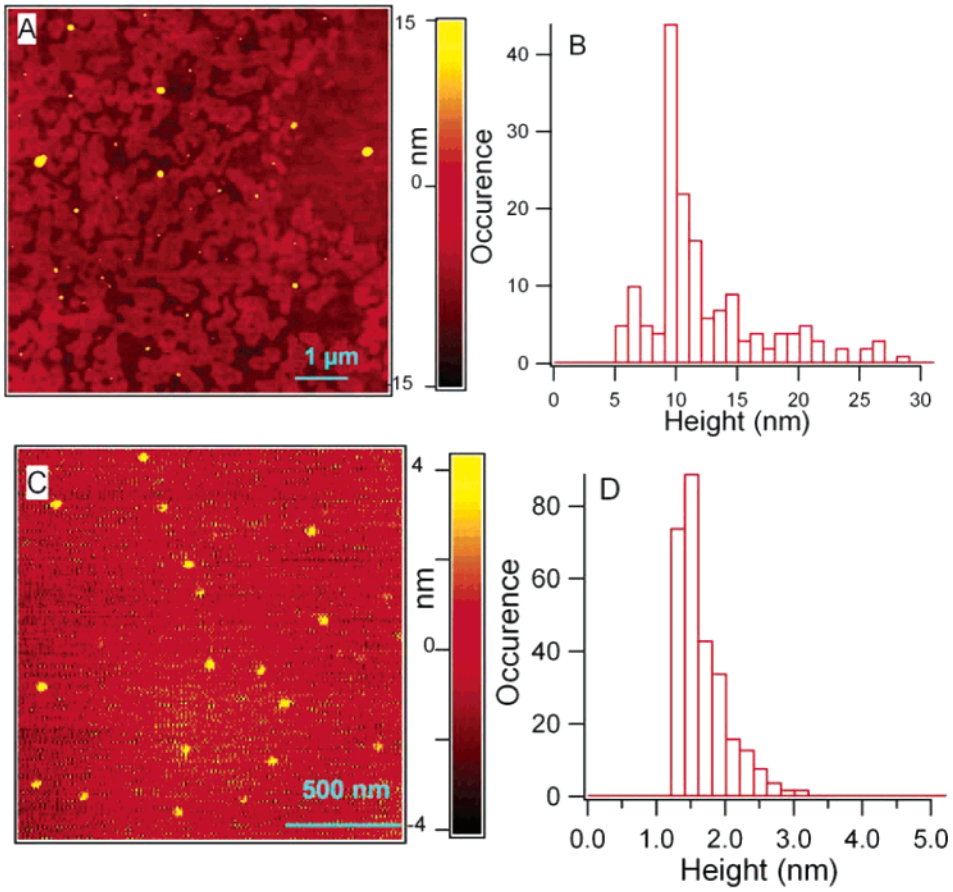

Figure 2. AFM image (A) of *z*-oriented CN-PPV nanoparticles on glass substrate produced by nebulization and (B) the particle heights distribution with a mean of 10.6 nm. The bottom panel shows the AFM image (C) of in plane oriented CN-PPV molecules deposited on mica surface and (D) the corresponding particle height distribution with a mean of 1.67 nm.

environment in the formation of highly organized oriented single conjugated polymer chains and the interplay with solution-phase morphologies.

Schwartz and co-workers[7] have clearly shown the correlation between "open" or "compact" solution-phase chain configurations on the luminescence properties of (macroscopic) solid films, and Huser and co-workers, in a similar spirit, have correlated (dry-state) single-molecule photophysical behavior with solvent effects.[23] In the case of *z*-oriented species formed from microdroplets of dilute polymer solution, the combination of uniform orientation (perpendicular to the glass substrate) and nearly 100% modulation depth in polarization anisotropy[25] suggests a very high degree of intramolecular organization. It was speculated that the effect of three-dimensional confinement in the microdroplet played a dominant role in this self-organization. However, under conditions of extremely rapid solvent evaporation (≤1 ms), the molecule will not have sufficient time to organize in response to the surface energy stress and will essentially become quenched in a configuration similar to its equilibrium solution-phase structure.

The observation of uniform dipole orientation from all the molecules in Figure 1A (prepared from toluene) suggests a high degree of structural order within each polymer chain, while no orientation or order (lack of emission patterns) was observed from samples prepared from DCM. Atomic force microscopy and polarization anisotropy measurements were carried out on the nanostructures, and the results point to high internal structural order within individual polymer chains[24,25] in the oriented species. Samples with *z*-oriented molecules are conveniently prepared from toluene solution, while *z*-oriented species are not observed for polymer samples nebulized from dichloromethane (DCM), as shown in Figure 1B. The fluorescence images of samples prepared from DCM appear mostly as simple diffraction-limited spots, while samples from toluene yield "doughnut"-like emission patterns indicative of *z*-oriented molecules. These results suggest that the difference in the emission patterns of CN-PPV (with similar results observed for MEH-PPV) prepared from toluene and DCM is a direct consequence of the polymer chain conformation in the solution phase.

In the cases examined here, droplet desolvation occurs on a very short time scale (<100 μs); the role of evaporating droplet in determining the morphology of individual polymer chains is minimal. Desolvation of the nebulized droplets occurs on a time scale that is shorter by more than 5 orders of magnitude than intrachain organization time scales.[29] Thus, the chain conformation observed in the dry state will closely resemble the solution-phase conformation. This implies that most of the order in the polymer chains in the oriented sample derives from the solution conformation, even though the high surface energy associated with the microdroplets may also have a role in determining the chain collapse. The number of antenna patterns and "doughnut"-like patterns decrease as a function of concentration, and larger chunks (which appear as diffraction-limited spots) of the polymer begin to appear at higher concentrations.

Figure 2 shows AFM surface height images for a *z*-oriented (A) and in-plane (B) CN-PPV sample along

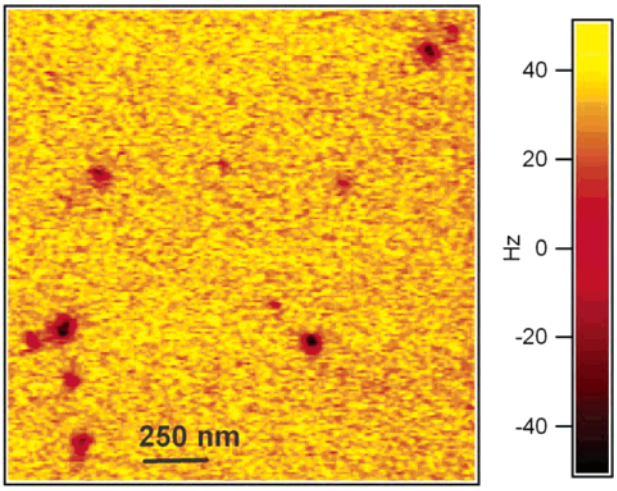

Figure 3. Electric force microscopy image of CN-PPV nanoparticles deposited on clean glass substrate acquired using EFM. The shift in cantilever frequency is a function of the charge on the nanoparticle. The dark regions denote net negative charge on the nanoparticles, and frequency shift indicates nominal excess charge of 2−8 electrons.

with the histogram of measured particle heights. Both samples were prepared under similar conditions using nebulization technique. For the *z*-oriented sample, the particle height distribution is sharply peaked around 10 nm, in close agreement with persistence length. These values are in good agreement with the persistence length of PPVs measured by dynamic light scattering techniques.[15] For CN-PPV nanoparticles that were oriented in the plane of the substrate (mica), the surface height distribution range from 1 to 3 nm with a mean of 1.67 nm. In both cases the individual particle images were tip radius tip radius limited (≈25 nm), thus obscuring $x-y$ structural information.

Electric force microscopy (EFM) was used to interrogate charge state (sign and magnitude) of nebulized nanostructures. Figure 3 shows an EFM image for *z*-oriented CN-PPV molecules prepared from toluene using the nebulization technique. The charge image was generated by measuring the shift in cantilever frequency; as a result of the long-range electrostatic forces, contrast in the image stems from the number and nature of charge carriers on the polymer chain. A negative shift in the cantilever resonance frequency due to charge interactions indicates, in this case, a net negative charge on the nanoparticle. This negative charge is generated during the ejection of the droplet from the orifice where the excess charges remain on the particle after solvent evaporation. Thus, we conclude that the particle orientation derives from an interaction with the nonprotonated SiO^- groups on the glass surface. Molecular dynamics simulations predict the localization of charges on the surface of the polymer chain, isolated from the emissive species, which is believed to be buried inside large number of chromophores folded back and forth.

Photophysical Properties of Oriented Single Molecules. Oriented nanostructures from single MEH-PPV and CN-PPV molecules, such as shown in Figure 1A, show a number of significantly enhanced photophysical properties relative to their thin-film counterparts. We observed narrow fluorescence emission (fwhm

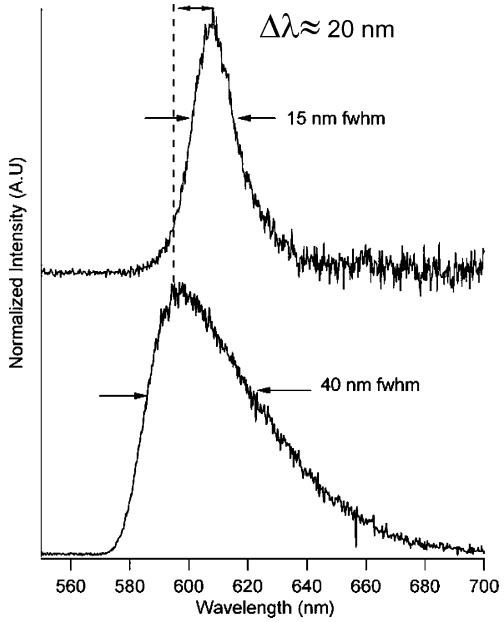

Figure 4. Fluorescence emission spectra of a *z*-oriented CNPPV single molecule (top) and a bulk sample of CNPPV (bottom). Spectral narrowing is observed in the case of oriented single molecule (15 nm fwhm) compared to the spectra of the bulk sample (40 nm fwhm). A red shift of ∼20 nm (0.1 eV) in peak of photoluminescence emission is also observed for the *z*-oriented single molecule compared to the bulk.

∼15 nm, typical) compared to the broad (∼40 nm) spectra from single molecules in neat film films. Figure 4 shows a comparison of the emission spectra from a single *z*-oriented CN-PPV molecule (top) and bulk CN-PPV sample (bottom). In the case of oriented MEH-PPV, samples showed strong evidence of energy funneling to a local chromophore inside the collapsed chain.[24] The polarization anisotropy measurements[25] indicate a collapsed polymer chain with the chromophores lying nearly parallel to each other.

We also observe significantly enhanced photostability of *z*-oriented MEH-PPV and CN-PPV relative to the bulk polymer or collapsed single chains oriented in the plane ($x-y$ plane) of the substrate. The oriented polymer molecules are photochemically stable up to a few hours under ambient conditions, while molecules that show transition moment orientation parallel to the substrate plane have photochemical lifetimes on the order of a few seconds. Parts A and B of Figure 5 show the intensity transients (fluorescence intensity vs time) of a CN-PPV single molecule oriented in the *z*-direction and in the substrate plane, respectively. The difference in photostability of the species lying in the substrate plane can be attributed to the electronic perturbations resulting from the sample−substrate interactions, while the sample−substrate interaction is minimal in the case of the oriented polymer molecule.

While luminescence properties give insight into the nature of emissive site, they do not provide explicit info on structure and organization. Barbara and co-workers[20] showed how polarization anisotropy measurements could be used to extract such information. The idea is to establish the connection between polartization anisotropy parameter (M) and structure of the molecule.

Figure 6 shows the intensity transient for the P−S polarization rotation cycle for a single *z*-oriented MEH-

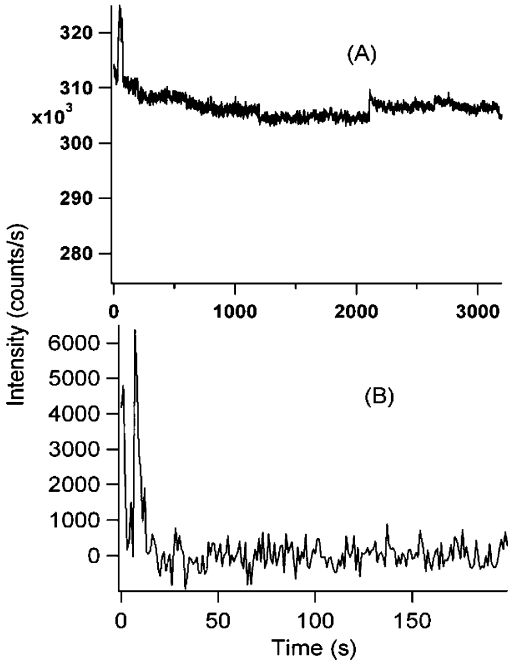

Figure 5. Fluorescence intensity transients of (A) a *z*-oriented molecule (B) and an in-plane (the substrate plane) oriented CN-PPV molecule acquired at ambient conditions. Note that the fluorescence signal from the *z*-oriented particle represented in (A) persists for >30× longer with count rates greater than 50× that of the in-plane species.

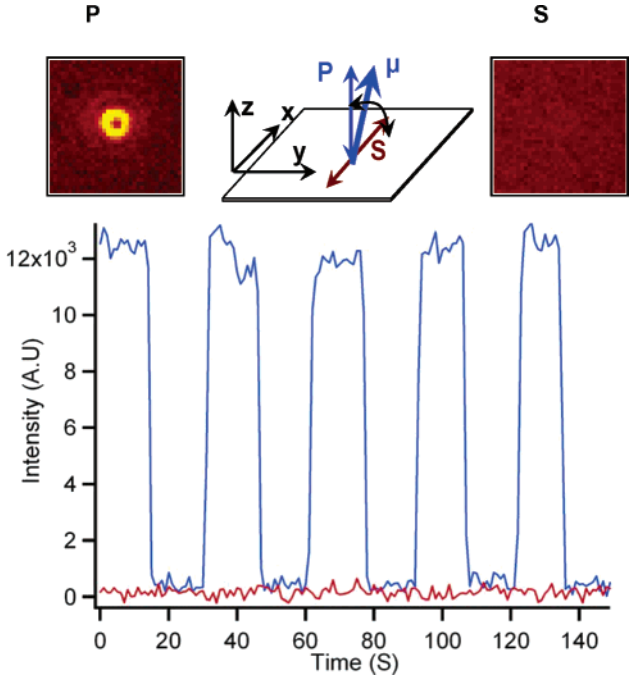

Figure 6. Background corrected intensity transient of a *z*-oriented MEH-PPV nanoparticle acquired under several P−S rotation cycles of the excitation polarization (blue). The average anisotropy parameter *M*, determined for five $\pi/2$ rotation cycle is 0.92. On the top panel are representative emission pattern image of the *z*-oriented nanoparticle under P and S polarizations. The two fluorescence images in the top panel are acquired under P (top left) and S polarizations (top right). Background reference is indicated in red.

PPV nanoparticle. The excitation polarization wasswitched between P and S every 15 s. For each pair ofP−S ($\pi/2$) polarization rotation, the anisotropy parameter was calculated using eq 1

$$M = \frac{I_p - I_s}{I_p + I_s} \quad (1)$$

where I_p and I_s are the fluorescence intensity in P and S polarizations, respectively.

Following Barbara and co-workers,[20] a mean value of 0.92 for *M* implies that the chromophores in the polymer chain are aligned approximately parallel to each other along the optic axis of the microscope, resulting in maximum absorption when the *z* component of the electric field is turned on (P polarization). This interpretation was further supported by analysis of time-resolved photon statistics that showed definitive evidence of a single localized emission site in these species,[26] indicating efficient energy transfer between the chromophores.

Fluorescence Correlation Spectra of MEH-PPV and CN-PPV. Fluorescence correlation spectroscopy (FCS) was used to measure diffusion coefficients of MEH-PPV and CN-PPV in different solvents. The diffusion coefficient is related to the hydrodynamic radii (R_h) through the Stokes−Einstein relationship. Analogous to dynamic (elastic) light scattering, FCS measures the fluorescence intensity fluctuations that derive from diffusion of molecules in to and out of a well-defined probe region. Solution-phase FCS measurements were carried out on a Nikon TE2000 inverted microscope operating in epi-illumination mode with an Ar^+ laser (514.5 nm; intensity ≈ 6 kW/cm^2) as excitation source. A high quantum efficiency avalanche photodiode (APD) was used for single photon counting and subsequent calculation of the correlation spectra. The signal from the APD was sent to a correlator card (ALV-6010, ALV-Laser, Germany), which determined the correlation function from the measured multichannel scalar data. A sample cuvette was constructed by attaching a glass cylinder to a cover glass with Torr Seal (Varian Vacuum Technologies). A rubber stopper was inserted into the top of the cuvette to prevent solvent evaporation during data collection. Solutions of different MEH-PPV and CN-PPV concentrations in toluene and THF ranging from 10^{-10} to 10^{-12} mol/L were used for the measurements.

The fluorescence correlation spectroscopic (FCS) measurement is a technique analogous to dynamic light scattering measurement and is based on the fluctuations in fluorescence intensity that arises from changes in the number of fluorescent molecules diffusing through the sampling volume.[30,31] The autocorrelation function of the fluorescence intensity as a function of time (1 ms dwell time) is connected to the diffusion coefficient by eq 2. The autocorrelation function for a single fluorescent species diffusing through a three-dimensional Gaussian intensity profile is given in ref 29

$$G(\tau) = \frac{1}{N}\left(1 + \frac{\tau}{\tau_D}\right)^{-1}\left(1 + \frac{\tau}{\omega^2\tau_D}\right)^{-1/2} \quad (2)$$

where τ is the time lag, $\tau = z_0/r_0$ (r_0 is the $1/e^2$ beam waist diameter, and z_0 is a parameter related to spherical aberration of the collection objective), *N* is the mean number of molecules in the probe volume, and τ_D is the characteristic diffusion time in which a probe molecule resides in the focal volume of the laser. The diffusion coefficient, *D*, is related to the characteristic diffusion time (τ_D) by the equation $D = r_0^2/4\tau_D$, where r_0 is beam waist diameter. The diffusion coefficient *D* is related to

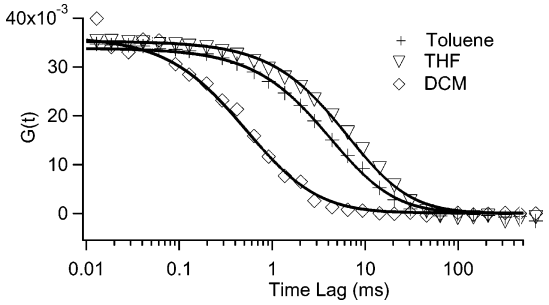

Figure 7. Fluorescence autocorrelation curves for freshly prepared solutions of MEH-PPV in DCM (◇), toluene (+), and THF (▽). The corresponding hydrodynamic radii are 2.6, 15.5, and 29.5 nm, respectively. The solid lines are fit to the data to eq 2.

the hydrodynamic radii, R_h, by the Stokes−Einstein relationship $R_h = kT/6\pi\eta_0 D$, where k is Boltzmann's constant, T is the temperature, and η_0 is the solvent viscosity. The mean number of fluorescent molecules, or molecular concentration, can be calculated from the initial correlation amplitude.

Figure 7 show autocorrelation curves for MEH-PPV solutions in DCM (◇), toluene (+), and THF (▽). The curves were fitted with single diffusion coefficient model. The hydrodynamic radii (R_h) of MEH-PPV in DCM, toluene, and THF from these curves were determined to be 2.6, 15.5, and 29.5 nm, respectively. Similar R_h values were found for CN-PPV in DCM (2.4 nm), toluene (23.4), and THF (44.5). That is, both MEH-PPV and CN-PPV adopt a more compact chain configuration in toluene relative to that in THF. The R_h values determined from analysis in DCM solution were unusually low (less than half of the persistence length) and are believed to result from an artifact resulting from multiple fluorescence events different segments of a single polymer molecule. The hydrodynamic radii also show a decrease with increase in solution concentration. We believe that this is an artifactual effect of fluorescence from multiple chains. The hydrodynamic radii of MEHPPV in toluene decreased from 14.7 , to 8.3, to 7.14 nm as the concentration is increased from 10^{-12}, to 10^{-11}, to 10^{-10} M. This is analogous to the dynamic light scattering data reported by Schwartz and co-workers where the reported hydrodynamic radii apparently decreased with concentration, an effect that was attributed to multiple scattering events from single chains. As shown by Chu et al.,[29] one expects, for a polydisperse sample, a distribution of hydrodynamic radii that is related to the molecular weight distribution, an effect that can be accounted for in more sophisticated methods such as CONTIN analysis.[32]

MD Simulation. To gain some insight into the structural orientation of MEH-PPV and CN-PPV, a combination of molecular dynamics and molecular mechanics (using the MM3 potential) carried out over nanosecond trajectories was used. The minimum-energy conformations of single molecule systems consisting of 14−70 monomers with tetrahedral defects located every seven monomers were determined for both MEH-PPV and CN-PPV. These simulations were performed for isolated single chain systems (no solvent) and with inclusion of solvent via the continuum model of the generalized Born approximation as well as with explicit solvent molecules (THF, toluene, dichloromethane). Figure 8 shows the progression of a typical molecular dynamics simulation. The initial configuration (Figure 8A) was obtained by propagating a MD

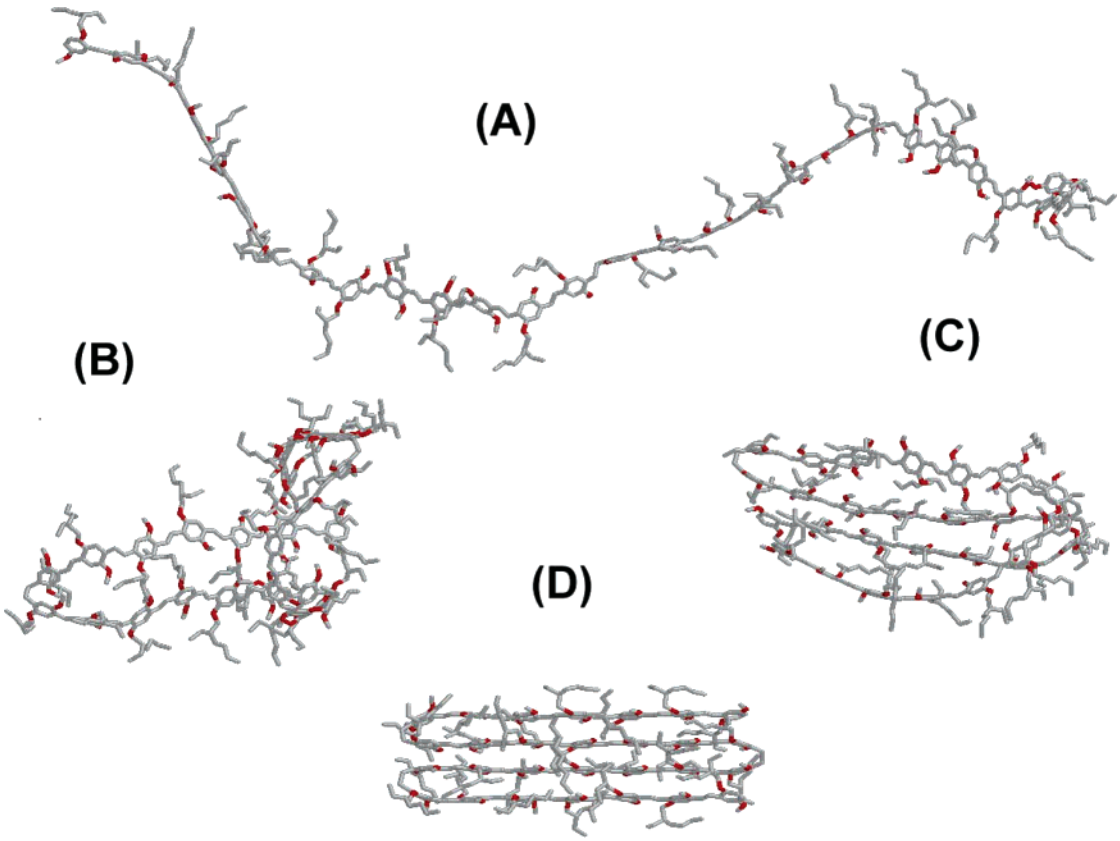

Figure 8. Snapshots of chain organization of a MEH-PPV oligomer in solution: (A) initial conformation; (B, C) conformations along a 1 ns simulation; (D) final optimized structure.

simulation of a linear chain of MEH-PPV consisting of 28 monomers and 3 tetrahedral defects at an elevated temperature (800 K) for short time. This allows the system to sample some of the possible phase space available from which an individual geometry is randomly selected. The next set of snapshots (Figure 8B,C) show how the MEH-PPV chain folds in a "bad" solvent (treated as a continuum dielectric) at the tetrahedral defects during the course of the trajectory. Determination of the lowest energy conformation (Figure 8D) was obtained by using a combination of simulated annealing and molecular mechanics without any solvent interactions (an attempt to emulate a dry particle as is obtained from the experimental generation), starting with the structure obtained from the MD simulation with solvent (Figure 8D). The interchain distance is $d = 3.7$ Å (determined between the two center chains), somewhat smaller than that determined by Conwell et al.[33] The difference in interchain distance is likely due to our use of slightly different potential energy functions (MM3 vs MM2) and the fact that we included chain folds, all of the atoms of the system explicitly for longer oligomer segments and larger number of "stacked oligomers" (some self-solvation is possible), and our accounting for the influence of solvent on the folding process and resulting geometry.

For CN-PPV of the same backbone length, very similar chain dynamics (although the rate of folding was ~2 times slower apparently due to the increased steric hindrance about the sp^3 C−C bond due to the CN groups) was found, and the minimum-energy configuration had an interchain distance of $d = 3.5$ Å (a clear decrease in the separation). Structural calculations using the MM3 potential have in general proven to be quite reliable, but in order to reduce any dependence on the type of potential we carried out extensive ab initio quantum chemistry calculations. The results obtained from these calculations are d(MEH-PPV) = 3.53−3.7 Å and d(CN-PPV) = 3.4−3.5 Å; however, these distances were determined for systems with only 14 monomers and 1 tetrahedral defect (these are relatively large many-body calculations) vs 28 monomers for the MM3 results. The general trend we have observed from the MM3 modeling is a decrease in the interchain separation as larger numbers of oligomer segments are added, indicating a self-solvation effect. In any case, the absolute numbers are probably not as accurate as the general trend of decreasing interchain separation for CN-PPV. The interchain distance reported from X-ray diffraction is $d = 3.56$ Å for MEH-PPV thin films, which is more in accord with our results from full ab initio quantum calculations carried out at the MP2 level of theory ($d = 3.53$ Å). One other interesting structural observation obtained from our simulations is that while PPV tends to form cofacial-planar geometries with a shift along the chain axis, MEH and CN-PPV tend to have a helical twist along the PPV backbone, with a larger angle for CN-PPV.

The effects of explicit solvent (full inclusion of all of the atoms) on the structure of MEH-PPV and CN-PPV were also examined. In these calculations, explicit solvent molecules were added to a MD box to achieve the appropriate density followed by aggressive energy minimization using molecular mechanics. To reduce the number of required solvent molecules, we started all calculations with a polymer molecule that had already been equilibrated in a continuum solvent simulation (such as that shown in Figure 8D). The final structures obtained were similar to those obtained for the continuum solvent systems but with some notable differences. For MEH-PPV the interchain distance increased to 4 Å in THF and 4.1 Å for DCM but decreased to 3.4 Å in toluene. The interchain distance for CN-PPV did not seem to be as strongly dependent on the solvent but did show an increased helical backbone structure.

Conclusions

The chain collapse and orientation of the single molecules were found to be highly influenced by the choice of the solvent. We have[24,25] shown how microdroplet techniques may be used to isolate single molecules of a conjugated polymer (MEH-PPV) to produce oriented nanostructures, resulting in enhanced photophysical properties. The collapsed, oriented single polymer molecules show spectral narrowing (~15 nm fwhm) with respect to the spectra of the bulk polymer (~40 nm fwhm) and enhanced photochemical stability relative to similar molecules lying in the substrate plane. The surface height measurements of *z*-oriented sample showed a height distribution maximum of 10.6 nm, in good agreement with the persistence length of the polymer reported in the literature. The height distribution peak for the in-plane oriented samples appear at 1.67 nm (much smaller than the persistence length), confirming their in-plane orientation. The charging of the nanoparticles was confirmed by electric force microscopy results, where the nanoparticles were shown to have net negative charges. Polarization anisotropy measurements resulted in anisotropy parameter of 0.92, indicating high internal structural order in the nanoparticle.

Samples nebulized from different solvents (toluene and DCM) were found to have different spatial fluorescence intensity patterns. Samples prepared from toluene appeared as toroidal patterns ("doughnut"-like) with a node in the center, indicating a perpendicular orientation of the transition dipole with respect to the substrate. Whereas, samples prepared from DCM appeared mostly as diffraction-limited spots, indicating random orientation of the transition dipoles within the molecule. We interpret this difference in emission patterns from single molecule polymer samples prepared from different solvents under similar conditions to mean that the chain collapse and the orientation of CN-PPV and MEH-PPV molecules are strongly dependent on the nature of the solvent. That is, molecules carry memory of the solution geometry into the dry state. This conclusion was supported by FCS measurements showing that MEH-PPV and CN-PPV adopt compact chain conformations in toluene relative to that in THF. Samples prepared from DCM show multichromophoric behavior, asserting the importance of solution chain conformations and sample preparation conditions on the collapse and orientation of the two conjugated polymers. The results obtained from MD simulations of MEH-PPV and CN-PPV also support the observations of collapsed single polymer molecules with highly organized internal structure. Simulations point to a well-extended polymer chain in DCM vs a collapsed structure in toluene for both MEH-PPV and CN-PPV. Thus, using microdroplet techniques, single, collapsed polymer molecules can be conveniently prepared from toluene than from other more polar solvents like THF or DCM. The enhanced photostability and the single quantum system behavior

of oriented single molecules of MEH-PPV and CN-PPV at ambient conditions have made them attractive candidates for possible use as stable, room temperature single photon sources and for nanophotonic applications.

Acknowledgment. This research was sponsored by the Division of Chemical Sciences, Office of Basic Energy Sciences, U.S. Department of Energy, under Contract DE-AC05-00OR22725 with Oak Ridge National Laboratory, managed and operated by UT-Battelle, LLC. Adosh Mehta acknowledges support of the ORNL Postdoctoral Research Program administered through Oak Ridge Institute of Science and Engineering (ORISE). Acknowledgment is also made to the donors of the Petroleum Research Fund, administered by the American Chemical Society, for partial support of this research (PRF# 38740-AC7).

References and Notes

(1) Burroughes, J. H.; Bradley, D. D. C.; Brown, A. R.; Marks, R. N.; Mackay, K.; Friend, R. H.; Burns, P. L.; Holmes, A. B. *Nature (London)* **1990**, *347*, 539−541.
(2) *Polymers for Photonic Applications I*; Springer: Berlin, 2002; Vol. 158.
(3) Heeger, A. J. *J. Phys. Chem. B* **2001**, *105*, 8475−8491.
(4) Hide, F.; DiazGarcia, M. A.; Schwartz, B. J.; Heeger, A. J. *Acc. Chem. Res.* **1997**, *30*, 430−436.
(5) Nguyen, T. Q.; Wu, J. J.; Doan, V.; Schwartz, B. J.; Tolbert, S. H. *Science* **2000**, *288*, 652−656.
(6) Nguyen, T. Q.; Yee, R. Y.; Schwartz, B. J. *J. Photochem. Photobiol. A: Chem.* **2001**, *144*, 21−30.
(7) Nguyen, T. Q.; Martini, I. B.; Liu, J.; Schwartz, B. J. *J. Phys. Chem. B* **2000**, *104*, 237−255.
(8) Nguyen, T. Q.; Schwartz, B. J. *J. Chem. Phys.* **2002**, *116*, 8198−8208.
(9) Collison, C. J.; Rothberg, L. J.; Treemaneekarn, V.; Li, Y. *Macromolecules* **2001**, *34*, 2346−2352.
(10) Nguyen, T. Q.; Doan, V.; Schwartz, B. J. *J. Chem. Phys.* **1999**, *110*, 4068−4078.
(11) Samuel, I. D. W.; Rumbles, G.; Collison, C. J.; Moratti, S. C.; Holmes, A. B. *Chem. Phys.* **1998**, *227*, 75−82.
(12) Zheng, M.; Bai, G. L.; Zhu, D. B. *J. Photochem. Photobiol. A: Chem.* **1998**, *116*, 143−145.
(13) Yan, M.; Rothberg, L. J.; Kwock, E. W.; Miller, T. M. *Phys. Rev. Lett.* **1995**, *75*, 1992−1995.
(14) Samuel, I. D. W.; Rumbles, G.; Collison, C. J. *Phys. Rev. B* **1995**, *52*, 11573−11576.
(15) Gettinger, C. L.; Heeger, A. J.; Drake, J. M.; Pine, D. J. *J. Chem. Phys.* **1994**, *101*, 1673−1678.
(16) Schwartz, B. J. *Annu. Rev. Phys. Chem.* **2003**, *54*, 141−172.
(17) Schaller, R. D.; Snee, P. T.; Johnson, J. C.; Lee, L. F.; Wilson, K. R.; Haber, L. H.; Saykally, R. J.; Nguyen, T. Q.; Schwartz, B. J. *J. Chem. Phys.* **2002**, *117*, 6688−6698.
(18) VandenBout, D. A.; Yip, W. T.; Hu, D. H.; Fu, D. K.; Swager, T. M.; Barbara, P. F. *Science* **1997**, *277*, 1074−1077.
(19) Yu, J.; Hu, D. H.; Barbara, P. F. *Science* **2000**, *289*, 1327−1330.
(20) Hu, D. H.; Yu, J.; Wong, K.; Bagchi, B.; Rossky, P. J.; Barbara, P. F. *Nature (London)* **2000**, *405*, 1030−1033.
(21) Huser, T.; Yan, M.; Rothberg, L. J. *Proc. Natl. Acad. Sci. U.S.A.* **2000**, *97*, 11187−11191.
(22) Yaron, D.; Moore, E. E.; Shuai, Z.; Bredas, J. L. *J. Chem. Phys.* **1998**, *108*, 7451−7458.
(23) Hollars, C. W.; Lane, S. M.; Huser, T. *Chem. Phys. Lett.* **2003**, *370*, 393−398.
(24) Kumar, P.; Mehta, A.; Dadmun, M. D.; Zheng, J.; Peyser, L.; Bartko, A. P.; Dickson, R. M.; Thundat, T.; Sumpter, B. G.; Noid, D. W.; Barnes, M. D. *J. Phys. Chem. B* **2003**, *107*, 6252−6257.
(25) Mehta, A.; Kumar, P.; Dadmun, M. D.; Zheng, J.; Dickson, R. M.; Thundat, T.; Sumpter, B. G.; Barnes, M. D. *Nano Lett.* **2003**, *3*, 603−607.
(26) Kumar, P.; Lee, T. H.; Mehta, A.; Sumpter, B. G.; Dickson, R. M.; Barnes, M. D. *J. Am. Chem. Soc.* **2004**, *126*, 3376−3377.
(27) Bartko, A. P.; Dickson, R. M. *J. Phys. Chem. B* **1999**, *103*, 11237−11241.
(28) Mehta, A.; Thundat, T.; Barnes, M. D.; Chhabra, V.; Bhargava, R.; Bartko, A. P.; Dickson, R. M. *Appl. Opt.* **2003**, *42*, 2132−2139.
(29) Chu, B.; Ying, Q. C.; Grosberg, A. Y. *Macromolecules* **1995**, *28*, 180−189.
(30) Magde, D.; Webb, W. W.; Elson, E. *Phys. Rev. Lett.* **1972**, *29*, 705-&.
(31) Magde, D.; Elson, E. L.; Webb, W. W. *Biopolymers* **1974**, *13*, 29−61.
(32) Provencher, S. W. *Makromol. Chem., Macromol. Chem. Phys.* **1979**, *180*, 201−209.
(33) Conwell, E. M.; Perlstein, J.; Shaik, S. *Phys. Rev. B* **1996**, *54*, R2308−R2310.

MA048917W